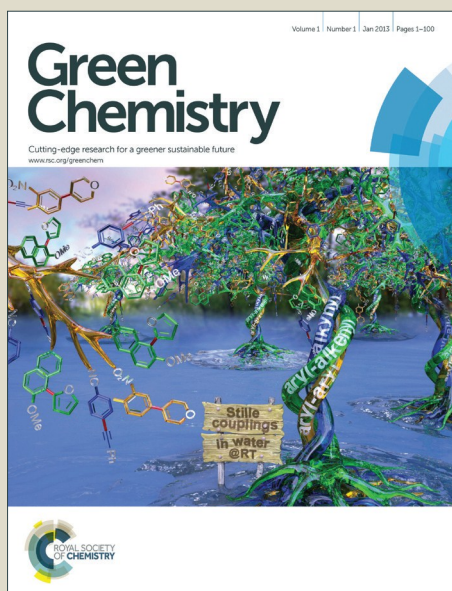


Green Chemistry

Accepted Manuscript



This article can be cited before page numbers have been issued, to do this please use: S. Zhu, X. Gao, Y. L. Zhu and Y. Li, *Green Chem.*, 2015, DOI: 10.1039/C5GC01766A.



This is an *Accepted Manuscript*, which has been through the Royal Society of Chemistry peer review process and has been accepted for publication.

Accepted Manuscripts are published online shortly after acceptance, before technical editing, formatting and proof reading. Using this free service, authors can make their results available to the community, in citable form, before we publish the edited article. We will replace this *Accepted Manuscript* with the edited and formatted *Advance Article* as soon as it is available.

You can find more information about *Accepted Manuscripts* in the [Information for Authors](#).

Please note that technical editing may introduce minor changes to the text and/or graphics, which may alter content. The journal's standard [Terms & Conditions](#) and the [Ethical guidelines](#) still apply. In no event shall the Royal Society of Chemistry be held responsible for any errors or omissions in this *Accepted Manuscript* or any consequences arising from the use of any information it contains.

1 **Tailored mesoporous copper/ceria catalysts for selective**
2 **hydrogenolysis of biomass-derived glycerol and sugar alcohols†**

3

4 Shanhui Zhu,^{*a} Xiaoqing Gao,^b Yulei Zhu,^{a,b} and Yongwang Li^{a,b}

5

6 ^a*State Key Laboratory of Coal Conversion, Institute of Coal Chemistry, Chinese*
7 *Academy of Sciences, Taiyuan 030001, PR China*

8 ^b*Synfuels China Co. Ltd., Taiyuan 030032, PR China*

9

10

11 *Corresponding author: *State Key Laboratory of Coal Conversion, Institute of Coal*
12 *Chemistry, Chinese Academy of Sciences, Taiyuan 030001, PR China.*

13 E-mail address: zhushanhui@sxicc.ac.cn

14 †Electronic supplementary information (ESI) available.

15

1 **Abstract:** The selective hydrogenolysis of sugar alcohols is a promising means to
2 produce valuable products from renewable biomass resources. The previous Cu-based
3 catalysts generally suffer from low activity and/or poor stability. We report the design
4 and fabrication of a tailored mesoporous copper/ceria catalyst by one-step solid-state
5 grinding-assisted nanocasting method. This new catalyst truly replicated the
6 morphology and mesoporous structure of the silica template, such as SBA-15 and
7 KIT-6. The characterization techniques strongly reflected that Cu^{2+} was successfully
8 substituted into the CeO_2 lattice and Cu nanoparticles were homogeneously dispersed
9 in the nanocomposite. This copper/ceria catalyst was highly active ($\text{TOF } 4.8 \text{ h}^{-1}$) and
10 stable for 300 h in glycerol hydrogenolysis to 1,2-propanediol. The excellent catalytic
11 performance is due to monodisperse Cu nanoparticles, strong interaction between Cu
12 and CeO_2 species, and tailored mesoporous structure.

13

1. Introduction

With declining fossil resources and rising CO₂ emissions, significant efforts have been devoted to the utilization of renewable resources, such as biomass.¹ One of the critical challenges in converting biomass into chemicals and fuels is to selectively cleave C–O linkages of highly functionalized molecules to lower the oxygen content. Sugar alcohols, such as glycerol, xylitol and sorbitol, are important platform molecules and can be readily available in huge amounts from biodiesel process or lignocellulose.²⁻⁴ Currently, deoxydehydration reaction has been effectively developed to eliminate two hydroxyl groups from vicinal diols to afford alkenes by various Re-based catalysts.⁵⁻⁷ For example, glycerol was mainly converted to ally alcohol while glucose was primarily yielded hexatriene over [CH₃ReO₃] via deoxydehydration method.⁵ Additionally, selective hydrogenolysis strategy offers a promising possibility because this approach can be used to high-yield produce a wide range of useful chemicals with low oxygen content. Moreover, hydrogenolysis holds the great potential to bridge currently available petroleum-technologies and future biomass refinery process.² For example, 1,2-propanediol (1,2-PDO) is an important precursor of polyester resin and pharmaceutical, which can be synthesized by selective hydrogenolysis of glycerol primary C–O bond.⁸⁻¹⁵ Huber et al.¹⁶ have reported the aqueous-phase hydrogenolysis of sorbitol to valuable alkanes and oxygenates with Pt/SiO₂-Al₂O₃. Liu et al.¹⁷ achieved high yields of ethylene glycol (EG, 32.4%) and 1,2-PDO (24.9%) from xylitol hydrogenolysis over Ru/C in the presence of Ca(OH)₂.

1 Among the catalysts for catalytic sugar alcohol hydrogenolysis, noble metal (e.g.,
2 Pt, Ru, Pd) have been employed extensively owing to their high activity and
3 stability.¹⁸⁻²⁸ Nevertheless, the expensive cost and limited availability of them have
4 necessitated the development of base catalysts with earth-abundant elements, such as
5 Fe, Ni and Cu. Copper-based catalysts, if designed elaborately, may be potential
6 alternative to precious metals for its intrinsic ability to cleave C–O bond
7 selectively.^{8,29} Nevertheless, copper nanoparticles are susceptible to irreversible
8 deactivation via sintering owing to the low melting point and Tammann temperature.³⁰
9 Some effective strategies to confine particle growth have been established, such as
10 alloying, regulating pore structure, fabricating core shell material, creating conformal
11 coatings by atomic layer deposition, increasing metal-support interaction and
12 optimizing interfacial area.³¹⁻³⁴ Recently, the encapsulation of individual nanoparticles
13 in morphologically well-defined inorganic tubes or shell has also gained considerable
14 interest owing to the outstanding thermal and chemical stability in catalysis.³⁵

15 Nanocasting is also called hard templating method, and has emerged as a highly
16 powerful approach for producing encapsulated nanoparticles in tailored non-silica
17 mesoporous tube or ordered pore.³⁶⁻³⁸ Although the mesoporous material from
18 nanocasting has lower orderliness than conventional soft templating method, it
19 endows abundant surface defects and is beneficial for improving the catalytic
20 performance. Tao et al.³² incorporated Au nanoparticles into mesoporous CeO₂
21 (mp-CeO₂) to synthesize highly active Au@mp-CeO₂ in water-gas shift reaction by
22 post-synthetic method; mp-CeO₂ was first made by nanocasting method in which

1 Ce(NO₃)₃·6H₂O was repeatedly impregnated into the pore of SBA-15. As a result of
2 the weak interaction between the metal ion precursors with Si–OH bonds during the
3 nanocasting process, it is challenging to fill the mesopores of silica template
4 completely. Therefore, the functionalization of silica template by organic groups can
5 be used to increase the interaction between the organic groups and metal ion precursor,
6 and maximize the quantity of metal ion precursor for good replication. Schüth et al.³⁹
7 have nanocast mesostructured Co₃O₄ with *Ia3d* symmetry from vinyl-functionalized
8 cubic mesoporous silica. Despite the great advances, the previous nanocasting
9 procedure needs multiple impregnation steps, using toxic solvent or surface
10 modification of template by functional agent.^{32,38,40-42} Herein, we report a novel
11 approach for the fabrication of copper-ceria mesoporous nanocomposite via
12 solid-state grinding-assisted nanocasting using ethanol as solvent. This one-step hard
13 template method not only simplifies the redundant procedures, but also provides a
14 green and versatile strategy to create mesoporous nanocomposite. This new
15 copper-ceria catalyst shows exceedingly high activity in glycerol hydrogenolysis and
16 exhibited excellent long-term stability for 300 h.

17

18 **2. Experimental**

19 **2.1 Catalyst preparation**

20 The copper-ceria mesoporous catalyst was prepared by solid-state
21 grinding-assisted nanocasting method. 1.903 g Cu(NO₃)₂·3H₂O (Sinopharm Chemical
22 Reagent Co., Ltd. (SCRC)), 5.05 g Ce(NO₃)₃·6H₂O (SCRC) and 2.0 g silica template

1 (including SBA-15 and KIT-6, Nanjing XFNANO Materials Technology Co., Ltd)
2 were mixed with 30 mL ethanol and grounded in a mortar at room temperature.
3 Subsequently, the mixture was dispersed to 150 mL ethanol solution at room
4 temperature under vigorous stirring for 24 h. After the ultrasonication for 30 min and
5 evaporation of ethanol at 80 °C, the sample was calcined at 500 °C for 4 h. Finally,
6 the silica template was treated three times by 2 M NaOH solution for 24 h. The
7 as-synthesized samples were labeled as CuCeSBA and CuCeKIT according to the
8 different silica template, respectively.

9 The mCeO₂ was fabricated using SBA-15 as a template with the method
10 described above. Cu/mCeO₂ was prepared by the impregnation of Cu(NO₃)₂·3H₂O
11 aqueous solution on mCeO₂. After impregnation, the catalyst was dried at 80 °C and
12 then calcined at 500 °C for 4 h.

13 CeO₂ nanorods (denoted as rCeO₂) were prepared by hydrothermal method based
14 on the reported procedures.⁴³ 4.5 mmol Ce(NO₃)₃·6H₂O was dissolved in 90 mL
15 NaOH solution (6 mol/L) under severe stirring for 10 min at room temperature. After
16 the mixture transferred into autoclave, hydrothermal treatment was performed at
17 100 °C for 24 h. Subsequently, the precipitates were collected by centrifugation, dried
18 at 80 °C overnight, and calcined at 400 °C for 4 h in static air. The Cu/rCeO₂ was
19 synthesized with similar method as Cu/mCeO₂.

20 **2.2 Catalyst characterization**

21 N₂ physisorption was measured at -196 °C on a Micromeritics TriStar II 3020
22 device after the catalysts were pretreated at 250 °C for 8 h in vacuum. BET surface

1 area was estimated from the desorption branch of adsorption-desorption isotherms.

2 Low angle X-ray diffraction (XRD) patterns were measured in D8/max-RA
3 X-ray diffractometer (Bruker, Germany). Wide angle XRD patterns were performed
4 on a D2/max-RA X-ray diffractometer (Bruker, Germany) using Cu K α radiation at 30
5 kV and 10 mA with a scanning speed (2θ) of 4 $^\circ$ /min. For *in situ* XRD measurement,
6 the sample remained in flowing H $_2$ at a flow rate of 30 cm 3 min $^{-1}$ and different preset
7 temperatures. Temperature ramping programs were set from 30 $^\circ$ C to 150, 200, 250,
8 300, 350, 400, 450 and 500 $^\circ$ C with a ramping rate of 5 $^\circ$ C min $^{-1}$. The XRD patterns
9 were recorded after the sample temperature reached the preset one for 30 min. The
10 full width at half maximum (FWHM) of Cu (1 1 1) diffraction at 2θ of 43.2 $^\circ$ was
11 chose to calculate Cu particle size according to Scherrer equation.

12 TEM and HRTEM were conducted on a JEM-2011F system electron
13 micro-scope at 200 kV equipped with a field emission gun. Prior to each test, the
14 sample was dispersed in ethanol under severe ultrasonication conditions for 20 min
15 and then deposited on copper grids coated with transparent carbon foil.

16 Raman spectroscopy was conducted on Renishaw-UV-vis Raman System 1000
17 using a multichannel air cooled CCD detector at room temperature. An Nd-Yag laser
18 operating at 532 nm was used as the exciting source with a power of 30 MW.

19 Temperature programmed reduction of H $_2$ (H $_2$ -TPR) was measured in an Auto
20 Chem. II 2920 apparatus (Mircromeritics, USA). At first, *ca.* 0.10 g sample was
21 charged into a quartz tube and pretreated in Ar at 150 $^\circ$ C for 30 min. After the catalyst
22 cooled to 30 $^\circ$ C, the Ar flow was changed into 10% H $_2$ -Ar mixed gas. Subsequently, a

1 cold trap of 2-propanol-liquid nitrogen slurry was employed to condense the water
2 vapor. Finally, the catalyst was heated from 30 °C to 500 °C at a ramp rate of
3 5 °C/min and meanwhile the consumption of hydrogen was recorded by a thermal
4 conductivity detector (TCD).

5 NH₃-TPD was performed in the same apparatus as H₂-TPR. In each run, 0.1 g
6 catalyst was pretreated in Ar at 400 °C for 20 min, cooled to 100 °C, and saturated
7 with pure NH₃ for 30 min. Subsequently, the sample was heated to 600 °C at a ramp
8 rate of 10 °C/min and the desorbed NH₃ was simultaneously monitored by a TCD
9 detector.

10 N₂O chemisorption was conducted in the same equipment as above. The catalyst
11 sample was loaded into a quartz tube and reduced according to the same H₂-TPR
12 procedure depicted as above. Subsequently, the catalyst was treated in a 10 vol.%
13 N₂O/N₂ flow (50 mL/min) for 30 min at 90 °C to oxidize the surface Cu⁰ to Cu₂O.
14 Finally, the sample was purged by Ar and cooled to 40 °C to start a new H₂-TPR
15 procedure. The Cu dispersion (D_{Cu}) was quantified by the following equation,

$$16 \quad D_{\text{Cu}} = 2Y/X \quad (\%)$$

17 where Y is the hydrogen consumption in the reduction of Cu₂O, and X is the
18 hydrogen consumption in the reduction of CuO.

19 XPS was conducted under an ultrahigh vacuum on a VG MultiLab 2000
20 spectrometer with Mg K α radiation and a multichannel detector. Prior to each test, the
21 catalyst was first reduced in H₂ at 250 °C for 2 h in an auxiliary pretreatment chamber
22 (glove box), and transferred into XPS sample holder. The obtained binding energies

1 were calibrated by the C1s peak at 284.6 eV as reference.

2 ICP optical emission spectroscopy (Optima2100DV, PerkinElmer) was
3 conducted to analyze the Cu contents of as-prepared catalysts.

4 Cu K-edge X-ray absorption spectroscopy (XAS) was measured in transmission
5 mode at the beam line of Beijing Synchrotron Radiation Facility (BSRF), Institute of
6 High Energy Physics (IHEP), Chinese Academy of Science (CAS). The XAS spectra
7 were analyzed on Athena XAS version 0.8.056. Background subtraction and
8 normalization were processed by fitting linear polynomials to the pre-edge and
9 post-edge region of absorption spectra, respectively. E_0 value was estimated according
10 to the maximum value in the first derivative of the edge region.

11 **2.3 Catalytic test**

12 All the catalytic tests were performed in a vertical fixed-bed reactor with an
13 ice-water trap. Typically, 2.0 g catalyst (20-40 mesh) was loaded into the constant
14 temperature section of the reactor with quartz sand fixed in both ends. Subsequently,
15 the catalyst was *in situ* reduced at 250 °C and atmospheric pressure for 2 h in flowing
16 H₂ (120 mL min⁻¹). After reduction, a 10 wt.% glycerol methanol solution was
17 continuously introduced into the reactor by a micro-pump along with co-feeding H₂
18 (120 mL min⁻¹) at 180 °C and 5.0 MPa. The liquid and gas products were cooled
19 down and collected in a gas-liquid separator immersed in an ice-water trap.

20 The liquid products of glycerol hydrogenolysis were analyzed by a gas
21 chromatography (GC, Ruihong chromatogram analysis Co., Ltd, China) equipped
22 with a capillary column (DB-WAX, 30 m × 0.32 mm) and a flame ionization detector

1 (FID). The tail gas was on-line analyzed by a GC (6890N, Agilent, USA) with a
2 capillary column (OV-101, 60 m × 0.25 mm) and a TCD. These products were also
3 identified by GC-MS (6890N, Agilent, USA). The carbon balance was checked in the
4 range of 95%-99%. The quantitative analysis was determined by the following
5 equations:

$$6 \quad \text{Conversion (\%)} = \frac{\text{moles of glycerol (in)} - \text{moles of glycerol (out)}}{\text{moles of glycerol (in)}} \times 100$$

$$7 \quad \text{Selectivity (\%)} = \frac{\text{moles of one product}}{\text{moles of all products}} \times 100$$

8 The liquid products of xylitol and sorbitol were analyzed by HPLC (Agilent
9 1260) with a shodex sugar SH-1821 column (300 mm × 8 mm, 5 μm) and a refractive
10 index detector (RID). The gas products were on-line analyzed by GC.

11

12 **3. Results and discussion**

13 **3.1 Catalyst synthesis and characterization**

14 Scheme 1 shows the preparation procedure of copper-ceria nanocomposite.
15 Before the nanocasting, Cu(NO₃)₂·3H₂O and Ce(NO₃)₃·6H₂O were manually ground
16 with the hard template (SBA-15 or KIT) in a mortar at room temperature to reach a
17 homogenous mixture. Subsequently, the mixture was dispersed into ethanol solution
18 under vigorous stirring. After the evaporation of ethanol, the mixture was calcined to
19 form mesoporous copper-ceria composite, and then the silica template was selectively
20 removed via chemical etching. Notably, solid-state grinding is important to introduce
21 the precursor species into the channels of mesoporous material and improve the
22 interaction between metal precursors and silica template. Thereby, this method does

1 not require repeated impregnation of active species into silica template. Additionally,
2 the synthesized CuCeSBA primarily consisted of short disordered nanorods without
3 solid-state grinding (Fig. S1†), implying the insufficient pore filling.

4 Compared to traditional methods,^{44,45} the Cu/CeO₂ nanocomposites *via*
5 nanocasting showed high BET surface area (Table 1). The BET surface area of
6 CuCeSBA was up to 160.9 m²g⁻¹, two times as high as that of Cu/mCeO₂. N₂
7 adsorption/desorption isotherms (Fig. S2†) presented typical hysteresis loops and
8 belonged to type IV, characteristic of mesoporous materials. The ordered mesoporous
9 structure was verified by low-angle XRD patterns (Fig. S3†). Both the two patterns
10 displayed a main strong peak at low 2θ value, which were assigned to the (1 0 0) and
11 (2 1 1) crystalline planes of the *p6mm* and *Ia3d* symmetries, respectively.³⁷ This
12 indicates the successful replication of CuCeSBA and CuCeKIT from the parent
13 SBA-15 and KIT-6.

14 As shown in Fig. 1, both the CuCeSBA and CuCeKIT displayed highly ordered
15 mesoporous structures. TEM images of CuCeSBA was indicative of a hexagonally
16 packed pore structure with an average diameter of about 7-8 nm, suggesting the
17 successful replication from the parent SBA-15. The high-resolution TEM image of
18 reduced CuCeSBA showed various nanocrystallites with well-defined lattice planes,
19 corroborating the high crystallinity of the pore walls. The smaller lattice strip of $d =$
20 0.208 nm in the pore structure belonged to Cu while in the nearby area another one of
21 $d = 0.310$ nm on the framework was assigned to (1 1 1) planes of fluorite CeO₂
22 phase,^{30,46} suggesting that Cu and CeO₂ were dispersed homogeneously in the pore

1 walls. In addition, the connecting bridges between two nanowires could also be
2 clearly observed, revealing the strong interaction between Cu and CeO₂ species.
3 Mesoporous CuCeKIT composite, consisting of nanowire arrays, was obtained with
4 the average pore diameter of 10 nm. The combination of HAADF-STEM (Fig. S4†)
5 and elemental EDX mapping (Fig. S5†) confirmed the homogenous distribution of Cu,
6 Ce and O in the mesoporous oxides, indicating that CuO and CeO₂ jointly constructed
7 the pore wall of mesoporous Cu/CeO₂ nanocomposite. However, Cu nanoparticles
8 were mainly embedded on the internal surface of mCeO₂ pore wall over Cu/mCeO₂
9 catalyst (Fig. S6†).

10 The mCeO₂ with good crystallization was obtained and supported by XRD
11 analysis (Fig. 2A). The typical diffuse diffraction peaks centered at 28.8°, 33.3°, 47.8°,
12 56.5°, 59.4° and 69.6° were indexed to the pure face-centered-cubic structure of (fcc)
13 CeO₂.³⁷ Only extremely weak CuO diffraction patterns at 35.6° and 38.8° were
14 detected over CuCeSBA and CuCeKIT,³⁰ suggesting that these Cu species were
15 highly dispersed or incorporation into the ceria lattice. Contrarily, the Cu/mCeO₂
16 exhibited obvious CuO diffraction patterns, reflecting the big Cu nanoparticles. The
17 H₂-TPR patterns (Fig. 2B) of CuCeSBA and CuCeKIT presented fairly symmetric
18 reduction peaks at low temperature, presumably implying that only one kind of
19 nano-sized Cu specie was located on these mesoporous composites because of the
20 formation of monodisperse CuO species. However, Cu/mCeO₂ showed a broad
21 reduction peak at high temperature, and contained at least two kinds of Cu species,
22 such as nano and bulk Cu species.

1 Strong interaction was convinced by the Raman spectroscopy result (Fig. 2C)
2 that the characteristic band at 462 cm^{-1} of F_{2g} vibration mode of CeO₂ lattice shifted
3 remarkably toward low wavenumber over CuCeSBA and CuCeKIT.³⁷ No shift was
4 observed over Cu/mCeO₂. In addition, a new broad band was observed at around
5 $500\text{-}660\text{ cm}^{-1}$ over CuCeSBA and CuCeKIT, which was ascribed to the structure
6 defects caused by the incorporation of heteroatom copper ions into ceria lattice.⁴⁴
7 These results from Raman were consistent well with the observation by XPS (Fig.
8 2D). There was strong electronic interaction between Cu and CeO₂ species in
9 mesoporous CuCeSBA(KIT) composites, as evidenced by the shift of Cu 2p peak
10 towards high binding energy. In comparison to Cu/mCeO₂, the Cu 2p peak of
11 CuCeSBA moved from 932.3 eV to 932.7 eV ,³⁰ verifying that the electron
12 transformed from Cu to CeO₂, and led to form Cu^{δ+}. The XPS data can also be
13 utilized to calculate the content of surface Cu atoms. Despite similar bulk Cu content
14 from ICP tests (Table 1), CuCeSBA afforded the highest surface Cu content. This was
15 indicative of the higher surface Cu dispersion of CuCeSBA, in well line with the
16 result based on N₂O chemisorption (Table 1). Compared to 3D cubic pore structure of
17 KIT, 2D hexagonal pore structure of SBA-15 facilitates to restrain CuO and CeO₂
18 nanoparticles, forms strong electronic interaction between CuO and CeO₂ species, and
19 results in the higher Cu dispersion. Additionally, the poor Cu dispersion of Cu/mCeO₂
20 could tentatively ascribed to the post-impregnation method that the pore confinement
21 of mesopores CeO₂ cannot effectively prevent the aggregation of Cu nanoparticles
22 during heat treatment.

1 Because the Raman spectra is a microdomain technique (area < 1 μm) and XPS
2 explores the catalyst surface (deep < 5 nm), both of them cannot fully reveal the
3 overall structural information, which can be replenished by XAS spectra. The Cu
4 K-edge XAS spectra of these Cu-based catalysts showed some interesting results in
5 Fig. 3A, B. The Cu-K-edge XANES definitely confirmed the ionic Cu^{2+} feature for all
6 the mesoporous copper-ceria catalysts. The related EXAFS spectra in R space (Fig.
7 3B) showed a strong contribution on the first shell of Cu–O bond. In bulk CuO, the
8 corresponding peak located at ca. 1.514 \AA .⁴⁷ For Cu/mCeO₂, the characteristic peak
9 remained and practically unchanged. Nevertheless, this peak underwent remarkable
10 shift over CuCeSBA and CuCeKIT. Specifically, the peak centered at 1.548 \AA over
11 CuCeSBA. This can be caused by the incorporation of CuO to CeO₂ lattice, verifying
12 strong interaction between CuO and CeO₂ species over CuCeSBA and CuCeKIT.

13 It is interesting to explore the thermal stability of CuCeSBA and Cu/mCeO₂; *in*
14 *situ* XRD (Fig. 4) was exhibited to monitor the Cu diffraction peaks in flowing H₂
15 upon different temperature. For CuCeSBA, the intensity and sharpness of Cu
16 diffraction peaks increased slowly in the range of 250- 600 $^{\circ}\text{C}$, and the average Cu
17 particle size determined by Scherrer equation only increased from 4.6 to 10.2 nm (Fig.
18 4C). Conversely, the Cu particle size sharply increased from 6.7 to 37.0 nm over
19 Cu/mCeO₂, reflecting the serious sintering and aggregation of copper nanoparticles
20 upon the same heat treatment. These Cu nanoparticles inside the channels of mCeO₂
21 cannot be sufficiently stabilized by the pore confinement effect at high temperature,
22 easily occur interparticle diffusion and subsequent agglomeration.

1 3.2 Catalytic performance

2 Selective hydrogenolysis of glycerol to 1,2-PDO is used to as a model reaction to
3 evaluate the catalytic behavior of mesoporous copper/ceria catalysts. As illustrated in
4 Fig. 5A, all the three catalysts obtained high 1,2-PDO selectivity (basically >90%)
5 because of the higher intrinsic ability to cleave C–O bond in preference to C–C bond
6 for Cu-based catalysts.^{13,30} All initial glycerol conversion reached or approached to
7 100% at low weight hourly space velocity (WHSV). Variations in glycerol conversion
8 within the series of mesoporous copper/ceria catalysts relate to the differences in
9 residence time with the change of WHSV. Of them, CuCeSBA gave the lowest
10 decline rate of glycerol conversion with the increasing WHSV, reflecting its highest
11 catalytic activity. Turnover frequency (TOF) can be utilized to reveal the intrinsic
12 active ability and the results are listed in Table 1. The TOF based on accessible
13 surface Cu atoms of CuCeSBA was calculated to be $4.8 \text{ mol}_{\text{glycerol}} \cdot \text{mol}_{\text{Cu(surf)}}^{-1} \cdot \text{h}^{-1}$ and
14 this value was much higher than that of Cu/mCeO₂. Under similar conditions, this
15 TOF was ca. 3~14 times as high as frequently reported Cu/SiO₂ catalysts,^{8,30,48}
16 unequivocally demonstrating the excellent activity of CuCeSBA. Fig. 5B displays a
17 comparison of long-term performance for the CuCeSBA and Cu/mCeO₂. The
18 CuCeSBA presented unprecedented catalytic behavior and was stable for 300 h.
19 Contrarily, significant deactivation of Cu/mCeO₂ occurred from 51 h to 171 h, and the
20 conversion decreased to 22.2% in the end.

21 The excellent catalytic activities presented by CuCeSBA and CuCeKIT
22 nanocomposites are partly ascribed to the formation of monodisperse Cu

1 nanoparticles and high surface Cu dispersion, which is attained through deliberate
2 design of the catalyst synthesis procedure. The solid-state grinding-assisted
3 hard-template method facilitates to form homogenous precursors' mixture, enhances
4 the interaction between metal precursors and silica surface during nanocasting,
5 promotes the infiltration of the precursors into the pore channels, and results in the
6 synthesis of homogeneously dispersed copper-ceria nanocomposites. Another
7 important factor is the presence of strong interaction and resultant CuO doped CeO₂
8 lattice. This can greatly affect planes, corner as well as edge atoms, correspondingly
9 modify both surface structure and electronic properties, and eventually form new
10 surface defects. These defects are coordinately unsaturated and endow high catalytic
11 ability for glycerol activation. Additionally, XPS test confirmed that electron transfer
12 from CeO₂ to Cu led to form Cu^{δ+}. The Cu^{δ+} species are favorable to enhance surface
13 Lewis acidity (Fig. S7[†]), promote the adsorption and polarization of hydroxyl groups
14 of glycerol,³⁰ and ultimately improve surface reaction rate. This can well explain the
15 enhanced TOF of CuCeSBA. Finally, the tailored mesoporous structure, which can be
16 controlled by various silica templates, appears to be another key to determine the
17 catalytic behavior. When using SBA-15 as template, the obtained copper-ceria
18 possesses a small pore size and large wall thickness, which is beneficial to confine
19 highly dispersed Cu nanoparticles and leads to enhanced reactivity.

20 Regarding the stability, the confined Cu nanoparticles inside the channels of
21 mesoporous mCeO₂ (Cu/mCeO₂) cannot effectively restrain their migration, Ostwald
22 ripening and sintering under long-term reaction. The significant aggregations of Cu

1 nanoparticles sharply decreased accessible Cu surface area, and thus led to its rapid
2 deactivation. Conversely, the existence of strong interaction together with Cu doped
3 CeO₂ lattice in CuCeSBA can restrict Cu nanoparticles migration, further limits their
4 growth via particle aggregation, and maintain high dispersion of copper species.
5 Therefore, CuCeSBA exhibited excellent thermal stability and rather steady
6 performance for glycerol hydrogenolysis under 180 °C and 5.0 MPa H₂ conditions.

7 We also prepared a comparable Cu/rCeO₂ catalyst, wherein Cu nanoparticles
8 anchored on the external surface of CeO₂ nanorods via post-impregnation. Owing to
9 the lack of pore confinement effect, the unconfined Cu nanoparticles became
10 seriously aggregated (Fig. S8†). Expectedly, very poor activity of Cu/rCeO₂ was
11 observed in glycerol hydrogenolysis, and even much lower than that of Cu/mCeO₂.
12 Under similar WHSV of 0.15 h⁻¹, 100% and 94.1% conversions of glycerol were
13 separately given over CuCeSBA and Cu/mCeO₂, while only 37.2% conversion was
14 obtained for Cu/rCeO₂. Therefore, sophisticated synthesis approach plays a key role
15 to achieve small and stable Cu nanoparticles and thereby excellent catalytic
16 performance. Our nanocasting method provides a homogenous copper-ceria
17 nanocomposite, wherein the copper has been successfully incorporated into ceria
18 lattices, and formed highly dispersed and robust Cu nanoparticles. The Cu
19 nanoparticles of CuCeSBA are smaller, more robust and active than that of Cu/mCeO₂,
20 despite the latter has pore confinement effect. More importantly, from the comparison
21 of the catalytic activity of various Cu/CeO₂ catalysts, we find that the metal doped
22 oxide nanocomposite is superior to the counterpart based on pore confinement effect,

1 and far superior to unconfined nanoparticles. These results also demonstrate that
2 highly active and stable Cu nanoparticles can be facily synthesized by nanocasting
3 method, by selectively incorporating metal species into the mesopore of SBA-15 via
4 solid-state grinding-assisted one-step impregnation after its calcination and sequential
5 etching.

6 To explore the versatility of mesoporous CuCeSBA, its catalytic performance
7 with different sugar alcohol substrates was evaluated and compared (Table 2).
8 1,2-PDO was predominantly converted to 1-propanol in 91.2% yield and a small
9 amounts of 2-propanol, implying that CuCeSBA preferentially cleaved primary C–O
10 bond. Similar trend was observed in the case of glycerol. This is related to the higher
11 barrier for the cleavage secondary C–O bond than that of primary one because of the
12 steric hindrance effect.⁴⁹ Hydrogenolysis of 1,3-propanediol (1,3-PDO) was
13 exclusively converted to 1-propanol in 98.2% selectivity. Regarding xylitol and
14 sorbitol, almost complete conversions were achieved over CuCeSBA, giving high
15 yields of valued products, including 1,2-PDO, ethylene glycol (EG) and glycerol. The
16 total yield of 1,2-PDO, EG and glycerol in xylitol hydrogenolysis was up to 71.7%,
17 which was even superior to the reported noble metal catalysts under similar
18 conditions.¹⁷ Additionally, base promoters like Ca(OH)₂ or KOH are usually required
19 to promote the cleavage of xylitol and sorbitol C–C bonds,^{17,50,51} while our CuCeSBA
20 did not need any extra additives. The CuCeSBA intrinsically contained large amounts
21 of acidic sites (Fig. S7†), which was also favorable to break C–C linkages of sorbitol
22 and xylitol.^{52,53} Notably, CuCeSBA showed powerful ability to cleave the C–C as

1 well as C–O bonds, and facilely converted sorbitol and xylitol to 1,2-PDO, EG and
2 glycerol under gentle conditions. However, it is difficult for CuCeSBA to efficiently
3 break C–C bonds of glycerol. Compared to xylitol and sorbitol, glycerol has a short
4 carbon chain and should require higher energy barrier to cleave C–C bond.

6 **4. Conclusions**

7 We have presented a facile and simple approach to fabricate mesoporous copper
8 doped ceria catalyst with one-step solid-state grinding-assisted nanocasting method.
9 This CuCeSBA nanocomposite exhibited excellent catalytic performance in the
10 hydrogenolysis of sugar alcohols owing to monodisperse Cu nanoparticles, strong
11 interaction between Cu and CeO₂ species, and tailored mesoporous structure.
12 Moreover, the incorporation of CuO into CeO₂ lattice provided spatial restriction on
13 copper nanoparticles, which can hinder their sintering under reaction conditions and
14 result in an enhanced stability. The Cu doped CeO₂ nanocomposite is superior to the
15 confined Cu/mCeO₂ counterpart, and far superior to unconfined Cu/rCeO₂
16 nanoparticles. It can be reasonably envisaged that such a low-cost, earth-abundant,
17 environmentally friendly and robust material will hold great potential for a wide range
18 of metal-catalyzed reactions.

20 **Acknowledgements**

21 We acknowledge the financial support of the National Natural Science Foundation of
22 China (21403269) and the Youth Innovation Promotion Association CAS (2015140).

1 We thank Dr. Pei Sheng for his help with EXAFS technique. Thanks are also given to
2 Beijing Synchrotron Radiation Facility.

3

4 **References**

- 5 1 S. Zhu, J. Wang and W. Fan, *Catal. Sci. Technol.* **2015**, *5*, 3845-3858.
- 6 2 A. M. Ruppert, K. Weinberg and R. Palkovits, *Angew. Chem. Int. Ed.*, 2012, **51**,
7 2564-2601.
- 8 3 D. Ten, Jeroen and U. Hanefeld, *ChemSusChem*, 2011, **4**, 1017-1034.
- 9 4 D. Roy, B. Subramaniam and R. V. Chaudhari, *ACS Catal.*, 2011, **1**, 548-551.
- 10 5 M. Shiramizu and F. D. Toste, *Angew. Chem.*, 2012, **124**, 8206-8210.
- 11 6 Y. Amada, N. Ota, M. Tamura, Y. Nakagawa and K. Tomishige, *ChemSusChem*,
12 2014, **7**, 2185-2192.
- 13 7 J. R. Dethlefsen and P. Fristrup, *ChemSusChem*, 2015, **8**, 767-775.
- 14 8 S. Zhu, X. Gao, Y. Zhu, Y. Zhu, H. Zheng and Y. Li, *J. Catal.*, 2013, **303**, 70-79.
- 15 9 M. G. Musolino, L. A. Scarpino, F. Mauriello and R. Pietropaolo, *ChemSusChem*,
16 2011, **4**, 1143-1150.
- 17 10 N. D. Kim, J. R. Park, D. S. Park, B. K. Kwak and J. Yi, *Green Chem.*, 2012, **14**,
18 2638-2646.
- 19 11 I. Gandarias, P. L. Arias, J. Requies, M. El Doukkali and M. B. Güemez, *J. Catal.*,
20 2011, **282**, 237-247.
- 21 12 S. Xia, R. Nie, X. Lu, L. Wang, P. Chen and Z. Hou, *J. Catal.*, 2012, **296**, 1-11.

- 1 13 E. S. Vasiliadou, T. M. Eggenhuisen, P. Munnik, P. E. de Jongh, K. P. de Jong and
2 A. A. Lemonidou, *Appl. Catal., B: Environ.*, 2014, **145**, 108-119.
- 3 14 Y. Nakagawa and K. Tomishige, *Catal. Sci. Technol.*, 2011, **1**, 179-190.
- 4 15 T. Miyazawa, Y. Kusunoki, K. Kunimori and K. Tomishige, *J. Catal.*, 2006, **240**,
5 213-221.
- 6 16 N. Li and G. W. Huber, *J. Catal.*, 2010, **270**, 48-59.
- 7 17 J. Sun and H. Liu, *Green Chem.*, 2011, **13**, 135-142.
- 8 18 I. Gandarias, P. L. Arias, J. Requies, M. B. Guemez and J. L. G. Fierro, *Appl.*
9 *Catal., B: Environ.*, 2010, **97**, 248-256.
- 10 19 C. Deng, X. Duan, J. Zhou, X. Zhou, W. Yuan and S. L. Scott, *Catal. Sci. Technol.*,
11 2015, **5**, 1540-1547.
- 12 20 W. Oberhauser, C. Evangelisti, R. P. Jumde, R. Psaro, F. Vizza, M. Bevilacqua, J.
13 Filippi, B. F. Machado and P. Serp, *J. Catal.*, 2015, **325**, 111-117.
- 14 21 J. Oh, S. Dash and H. Lee, *Green Chem.*, 2011, **13**, 2004-2007.
- 15 22 F. Mauriello, H. Ariga, M. G. Musolino, R. Pietropaolo, S. Takakusagi and K.
16 Asakura, *Appl. Catal., B: Environ.*, 2015, **166-167**, 121-131.
- 17 23 K. L. Deutsch, D. G. Lahr and B. H. Shanks, *Green Chem.*, 2012, **14**, 1635-1642.
- 18 24 S. Zhu, X. Gao, Y. Zhu and Y. Li, *J. Mol. Catal. A: Chem.*, 2015, **398**, 391-398.
- 19 25 S. Zhu, Y. Zhu, S. Hao, H. Zheng, T. Mo and Y. Li, *Green Chem.*, 2012, **14**,
20 2607-2616.
- 21 26 R. Arundhathi, T. Mizugaki, T. Mitsudome, K. Jitsukawa and K. Kaneda,
22 *ChemSusChem*, 2013, **6**, 1345-1347.

- 1 27 P. K. Vanama, A. Kumar, S. R. Ginjupalli and V. R. C. Komandur, *Catal. Today*,
2 2015, **250**, 226-238.
- 3 28 J. Ge, Z. Zeng, F. Liao, W. Zheng, X. Hong and S. C. E. Tsang, *Green Chem.*,
4 2013, **15**, 2064-2069.
- 5 29 E. S. Vasiliadou, V. L. Yfanti and A. A. Lemonidou, *Appl. Catal., B: Environ.*,
6 2015, **163**, 258-266.
- 7 30 S. Zhu, X. Gao, Y. Zhu, W. Fan, J. Wang and Y. Li, *Catal. Sci. Technol.*, 2015, **5**,
8 1169-1180.
- 9 31 X. Jin, L. Dang, J. Lohrman, B. Subramaniam, S. Ren and R. V. Chaudhari, *ACS*
10 *Nano*, 2013, **7**, 1309-1316.
- 11 32 C. Wen, Y. Zhu, Y. Ye, S. Zhang, F. Cheng, Y. Liu, P. Wang and F. Tao, *ACS*
12 *Nano*, 2012, **6**, 9305-9313.
- 13 33 G. Prieto, M. Shakeri, K. P. de Jong and P. E. de Jongh, *ACS Nano*, 2014, **8**,
14 2522-2531.
- 15 34 F. Wang, R. Shi, Z.-Q. Liu, P.-J. Shang, X. Pang, S. Shen, Z. Feng, C. Li and W.
16 Shen, *ACS Catal.*, 2013, **3**, 890-894.
- 17 35 H. Yue, Y. Zhao, S. Zhao, B. Wang, X. Ma and J. Gong, *Nat. Commun.*, 2013, **4**,
18 2339.
- 19 36 Y. Ren, Z. Ma and P. G. Bruce, *Chem. Soc. Rev.*, 2012, **41**, 4909-4927.
- 20 37 H. Yen, Y. Seo, S. Kaliaguine and F. Kleitz, *Angew. Chem. Int. Ed.*, 2012, **51**,
21 12032-12035.

- 1 38 H. Yen, Y. Seo, R. Guillet-Nicolas, S. Kaliaguine and F. Kleitz, *Chem. Commun.*,
2 2011, **47**, 10473-10475.
- 3 39 F. Schüth, *Adv. Mater.*, 2005, **17**, 53-56.
- 4 40 A. Ruplecker, F. Kleitz, E.-L. Salabas and F. Schüth, *Chem. Mater.*, 2007, **19**,
5 485-496.
- 6 41 P. Djinić, J. Batista and A. Pintar, *Catal. Today*, 2009, **147S**, S191-S197.
- 7 42 H. Tüysüz, E. L. Salabaş, E. Bill, H. Bongard, B. Spliethoff, C. W. Lehmann and F.
8 Schüth, *Chem. Mater.*, 2012, **24**, 2493-2500.
- 9 43 R. Si and M. Flytzani-Stephanopoulos, *Angew. Chem. Int. Ed.*, 2008, **47**,
10 2884-2887.
- 11 44 W.-W. Wang, P.-P. Du, S.-H. Zou, H.-Y. He, R.-X. Wang, Z. Jin, S. Shi, Y.-Y.
12 Huang, R. Si, Q.-S. Song, C.-J. Jia and C.-H. Yan, *ACS Catal.*, 2015, **5**,
13 2088-2099.
- 14 45 A. Aranda, E. Aylon, B. Solsona, R. Murillo, A. M. Mastral, D. R. Sellick, S.
15 Agouram, T. Garcia and S. H. Taylor, *Chem. Commun.*, 2012, **48**, 4704-4706.
- 16 46 L. Wan, X. Cui, H. Chen and J. Shi, *Mater. Lett.*, 2010, **64**, 1379-1382.
- 17 47 J. S. Elias, M. Risch, L. Giordano, A. N. Mansour and Y. Shao-Horn, *J. Am. Chem.*
18 *Soc.*, 2014, **136**, 17193-17200.
- 19 48 Z. W. Huang, F. Cui, H. X. Kang, J. Chen, X. Z. Zhang and C. G. Xia, *Chem.*
20 *Mater.*, 2008, **20**, 5090-5099.
- 21 49 M. R. Nimlos, S. J. Blanksby, X. Qian, M. E. Himmel and D. K. Johnson, *J. Phys.*
22 *Chem. A*, 2006, **110**, 6145-6156.

- 1 50 L. Zhao, J. H. Zhou, Z. J. Sui and X. G. Zhou, *Chem. Eng. Sci.*, 2010, **65**, 30-35.
- 2 51 M. Banu, S. Sivasanker, T. M. Sankaranarayanan and P. Venuvanalingam, *Catal.*
3 *Commun.*, 2011, **12**, 673-677.
- 4 52 D. Liang, C. Liu, S. Deng, Y. Zhu and C. Lv, *Catal. Commun.*, 2014, **54**, 108-113.
- 5 53 I. M. Leo, M. L. Granados, J. L. G. Fierro and R. Mariscal, *Chin. J. Catal.*, 2014,
6 **35**, 614-621.
- 7



1

2 **Scheme 1** The procedure of one-step solid-state grinding-assisted nanocasting for the

3

preparation of mesoporous copper-ceria nanocomposite.

4

1 **Table 1** The physicochemical properties and turnover frequency (TOF) of various

2 Cu-based catalysts

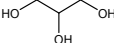
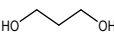
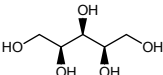
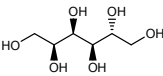
Catalyst	S_{BET} (m^2g^{-1}) ^a	Pore volume (cm^3g^{-1}) ^a	Pore size (nm) ^a	Cu content (wt%) ^b	Surface Cu content (at%) ^c	Cu dispersion (%) ^d	TOF (h^{-1}) ^e
CuCeSBA	160.9	0.332	7.8	16.59	17.5	24.9	4.8
CuCeKIT	86.8	0.224	10.1	17.74	12.7	20.2	4.1
Cu/mCeO ₂	69.3	0.193	11.1	16.63	8.5	13.8	3.4

^aDetermined by N₂ physisorption. ^btested by ICP. ^ccalculated based on XPS. ^ddetermined by N₂O chemisorption. ^eTOF is moles of converted glycerol per mole of surface Cu sites and per hour. The reaction conditions were chosen to determine the rate below 20% conversion.

3

1 **Table 2** Catalytic performance for the hydrogenolysis of different substrates over

2 CuCeSBA catalyst^a

Entry	Substrate	Conversion (%)	Product selectivity (%)
1	 glycerol	100	1,2-PDO (96.9%)
2	 1,2-PDO	100	1-propanol (91.2%), 2-propanol (7.8%)
3	 1,3-PDO	93.5	1-propanol (98.2%)
4 ^b	 xylitol	100	1,2-PDO (41.5%), EG (24.5%), glycerol (5.7%)
5 ^b	 sorbitol	99.2	1,2-PDO (32.4%), EG (10.8%), glycerol (6.8%)

^aReaction conditions: 180 °C, 5.0 MPa, H₂/glycerol = 100:1 (molar ratio); ^b220 °C.

3

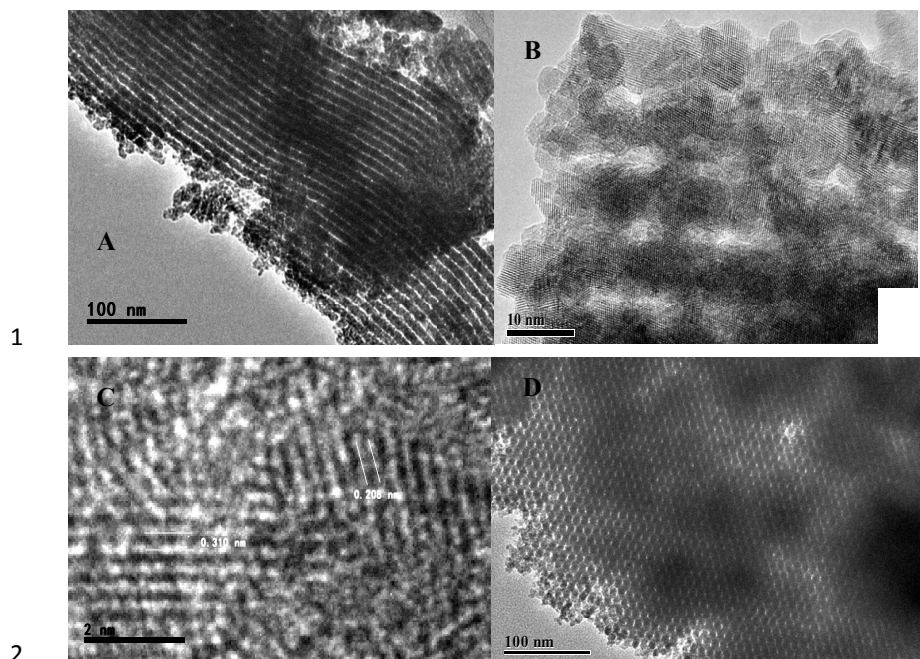


Fig. 1 Representative TEM or HRTEM images of (A) CuCeSBA, (B) CuCeSBA, (C) CuCeSBA, (D) CuCeKIT.

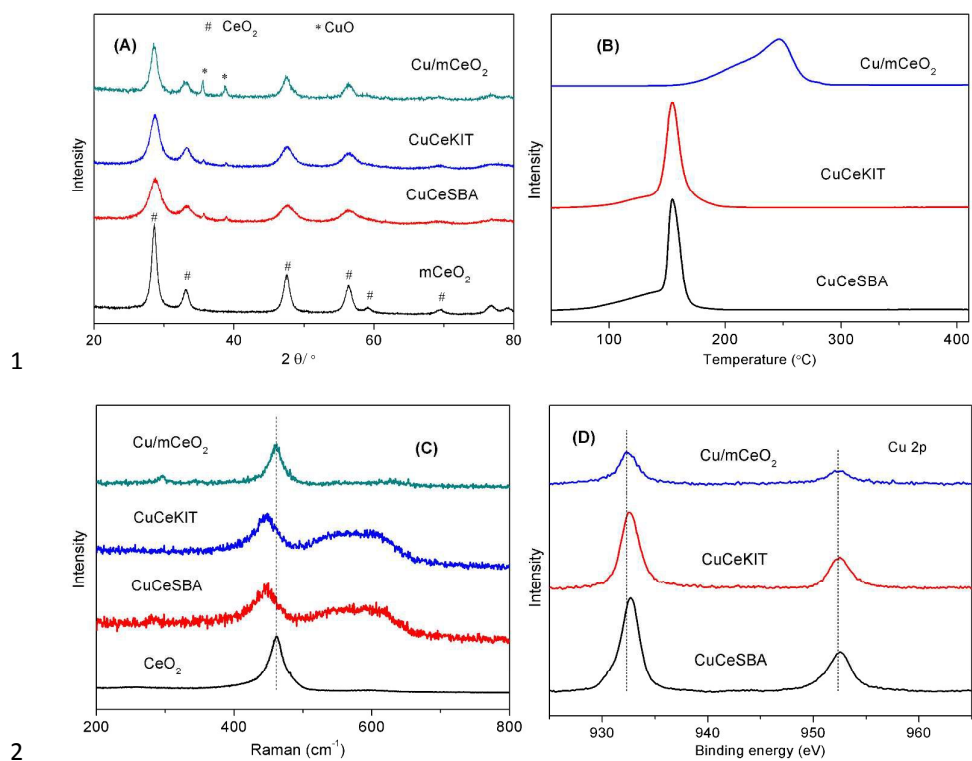
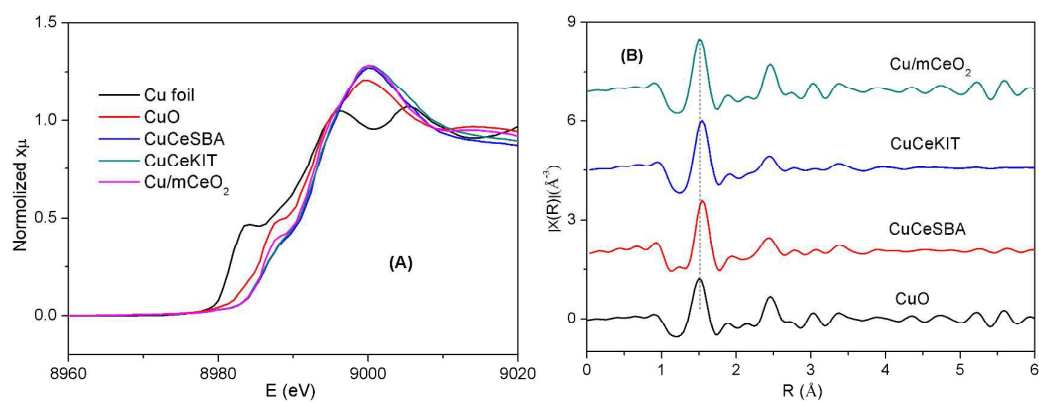


Fig. 2 (A) XRD, (B) H₂-TPR and (C) Raman spectra of calcined Cu-based catalysts;
(D) Cu 2p XPS photoemission peaks of reduced Cu-based catalysts.

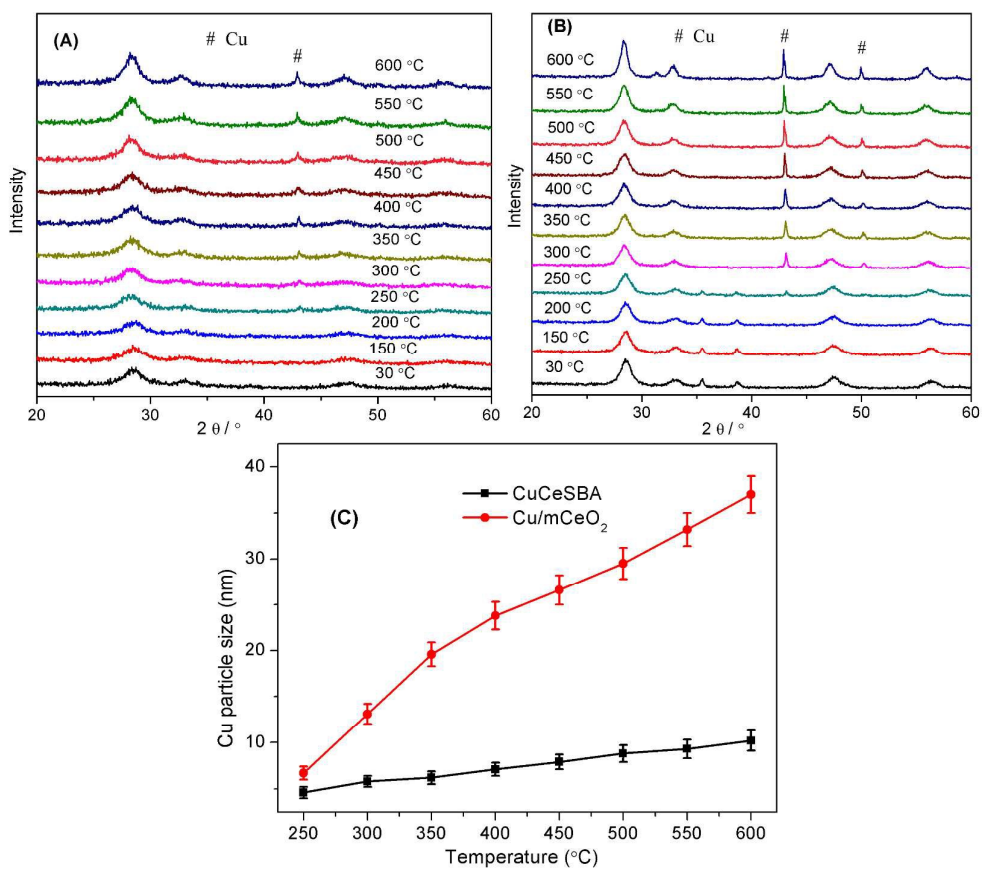
1



2

3 **Fig. 3** (A) Cu K-edge XANES spectra and (B) the magnitude of the k^2 -weighted

4 Fourier transform of the EXAFS of Cu-based catalysts.

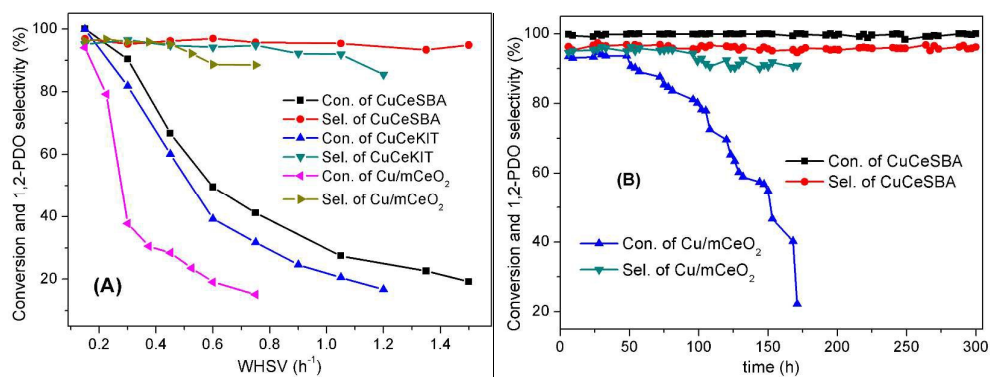


1

2

3 **Fig. 4** *In situ* XRD patterns of (A) CuCeSBA and (B) Cu/mCeO₂ as a function of
 4 thermal treatment at various temperature in flowing H₂; (C) Average Cu particle size
 5 as a function of treating temperature.

6



1

2 **Fig. 5** (A) The dependence of glycerol conversion and 1,2-PDO selectivity with

3 WHSV over various Cu-based catalysts; Reaction conditions: 180 °C, 5.0 MPa,

4 H₂/glycerol = 100:1 (molar ratio). (B) The long-term performance of CuCeSBA and5 Cu/mCeO₂ catalysts. Reaction conditions: 180 °C, 5.0 MPa, WHSV = 0.15 h⁻¹,6 H₂/glycerol = 100:1 (molar ratio).

7

Graphic abstract

Mesoporous copper/ceria catalysts, prepared via grinding-assisted nanocasting method, presented excellent activity and stability for hydrogenolysis of biomass-derived sugar alcohols.

